Temperature dependence of He($2\,^3P_J$) reactions: Collision-induced mixing and conversion to $He_2(b\,^3\Pi_g)$ molecules

X. Zhao, P. A. Soletsky, W. H. Bryan, F. B. Dunning, and G. K. Walters
Department of Physics and the Rice Quantum Institute, Rice University, P.O. Box 1897, Houston, Texas 77251
(Received 25 June 1993)

The rate coefficients for mixing between He($2\,^3P_{J,M_J}$) levels during collisions with ground-state helium atoms and for conversion of He($2\,^3P_J$) atoms to $He_2(b\,^3\Pi_g)$ molecules via three-body reactions in helium gas have been investigated over the temperature range 1.6–300 K. The measured rate coefficients for collisionally induced P-state mixing decrease slowly with decreasing temperature, from $(1.8\pm0.5)\times10^{-9}$ $cm^3\,s^{-1}$ at 300 K to $(4.5\pm0.5)\times10^{-10}$ $cm^3\,s^{-1}$ at 4.2 K. The rate coefficients for the production of $He_2(b\,^3\Pi_g)$ molecules via three-body reactions are observed to increase with decreasing temperature and are described by the relation $k_P\cong(2.5+267T^{-1})\times10^{-32}$ $cm^6\,s^{-1}$. This behavior, which is very different from that noted in earlier studies of the conversion of He($2\,^3S_1$) atoms to $He_2(a\,^3\Sigma_u^+)$ molecules through three-body reactions, suggests that the reaction is not thermally activated.

PACS number(s): 34.50.−s

Interactions between atoms in ground and low-lying excited states, and the collisional processes that influence excited-state lifetimes in helium gas have been the subjects of numerous investigations over many years. In particular, relatively large populations ($\gtrsim10^{10}$ cm^{-3}) of helium atoms in the $2\,^3S_1$ state can easily be produced, and their collisional properties have been extensively studied [1–13]. The He($2\,^3S_1$)-He($1\,^1S_0$) interaction potential is very unusual in that the competition between the $He_2^+(1\sigma_g^2 1\sigma_u)$ core attraction and the He($1s^2$)+He($1s2s$) exchange repulsion gives rise to a sizable (~60 meV) repulsive barrier at intermediate nuclear separations (~3 Å) before yielding to the strongly attractive $He_2(a\,^3\Sigma_u^+)$ molecular well at smaller distances (~1 Å) [1],[10–13]. The presence of the repulsive barrier has been shown to affect dramatically the temperature dependences of He($2\,^3S_1$) diffusion in helium gas [8] and the rate for metastability exchange in He($2\,^3S_1$)-He($1\,^1S_0$) collisions [5–7], and also is responsible for the formation of stable microscopic voids ("bubbles") surrounding He($2\,^3S_1$) atoms in liquid helium [14,15]. The existence of a barrier also means that the conversion of He($2\,^3S_1$) atoms to $He_2(a\,^3\Sigma_u^+)$ molecules via the three-body reaction,

$$\mathrm{He}(2\,^3S_1)+2\mathrm{He}(1\,^1S_0)\rightarrow\mathrm{He}_2(a\,^3\Sigma_u^+)+\mathrm{He}(1\,^1S_0)\ , \qquad (1)$$

must be thermally activated. Surprisingly, recent experiments in this laboratory have revealed that the effective activation energy decreases at low temperatures, suggesting that, for certain reaction geometries, the barrier can be significantly lowered by the presence of the third body [16].

In this paper we report measurements of the temperature dependence of the rate coefficients for mixing between different He($2\,^3P_{J,M_J}$) sublevels in collisions with ground-state helium atoms via the reaction,

$$\mathrm{He}(2\,^3P_{J,M_J})+\mathrm{He}\rightarrow\mathrm{He}(2\,^3P_{J',M_J'})+\mathrm{He}\ . \qquad (2)$$

Knowledge of collisional mixing rates is important in the interpretation and further development of He($2\,^3S_1$) optical pumping techniques for producing spin-polarized electron beams [17] and spin-polarized ^{3}He targets for nuclear scattering experiments [18], and for studies of low-temperature ^{3}He and ^{3}He-^{4}He quantum fluids [19]. In addition, we have investigated the temperature dependence for conversion of He($2\,^3P_J$) atoms to $He_2(b\,^3\Pi_g)$ molecules through three-body reactions in helium gas of the type

$$\mathrm{He}(2\,^3P_J)+2\mathrm{He}(1\,^1S_0)\rightarrow\mathrm{He}_2(b\,^3\Pi_g)+\mathrm{He}(1\,^1S_0)\ . \qquad (3)$$

Reactions (1) and (3) are among the simplest of all ternary reactions and are amenable to investigation over an extraordinarily wide range of temperatures. Thus a thorough study of these systems promises new insights regarding ternary reaction dynamics. Further, spectroscopic studies of He($2\,^3P_J$) atoms in liquid helium suggest that, like He($2\,^3S_1$) atoms, they repel the ground-state fluid and are surrounded by a (nonspherical) "bubble" that approximately mirrors the probability density of the $2p$ orbital [15]. This would imply the existence of a repulsive barrier in the He($2\,^3P_J$)-He($1\,^1S_0$) interaction potential at intermediate nuclear separations, as for the He($2\,^3S_1$)-He($1\,^1S_0$) interaction. However, the exchange repulsion, and thus interaction potential, should depend strongly on the collision geometry, being smallest when the internuclear axis is in the nodal plane of the $2p$ orbital where the p-electron probability density is a minimum. The present data show that reaction (3) does not require thermal activation, indicating that, at least for collisions near the $2p$ nodal plane, exchange repulsion is insufficient to produce a barrier.

Studies of reactions involving He($2\,^3P_J$) atoms, which

are typically produced by photoexcitation of He($2\,^3S_1$) atoms, have been hampered by the lack of a convenient tunable source of monochromatic radiation at the wavelengths (~ 1.083 μm) required for exciting $2\,^3S_1 \rightarrow 2\,^3P_J$ transitions, and by the short radiative lifetime ($\sim 10^{-7}$ s) of the $2\,^3P_J$ states, which limits attainable He($2\,^3P_J$) densities. In the present work, rate constants for P-state mixing [reaction (2)] were derived through line-shape analysis from measurements, undertaken using a Ti:sapphire laser, of the absorption profiles for $2\,^3S_1 - 2\,^3P_J$ transitions in a weak rf discharge in helium gas. Rate constants for three-body conversion [reaction (3)] were obtained by using the laser to partially saturate a particular $2\,^3S_1 - 2\,^3P_J$ transition and monitoring the decay of the resulting radiation-coupled $2\,^3S_1/2\,^3P_J$ population in the afterglow of a pulsed rf discharge.

The present apparatus is shown schematically in Fig. 1. Its central component is a cylindrical Pyrex sample cell that was initially prepared by baking and electrical-discharge cleaning and then filled with helium gas to the desired density. For measurements at low temperatures the cell was immersed in either liquid nitrogen or liquid helium, and temperatures below the 4.2-K liquid-helium boiling point at atmospheric pressure were achieved by pumping the vapor to reduce its pressure. Helium atoms in the cell were excited to the $2\,^3S_1$ state by igniting a weak electrodeless 3-MHz rf discharge. Care was taken to ensure that the rf discharge power was low enough to avoid heating the sample gas significantly.

Line shapes for the $2\,^3S_1 - 2\,^3P_J$ transitions were measured using a single-mode, frequency-stabilized Coherent CR899-21 Ti:sapphire laser, which was optimized for operation at 1.083 μm, by scanning the laser output frequency and recording the corresponding absorption spectrum. The expected line shape is a convolution of a Gaussian resulting from Doppler (inhomogeneous) broadening,

$$g_G(\omega,\omega_0)=\left[\frac{4\ln 2}{\pi}\right]^{1/2}\frac{1}{\Delta\omega_G}\exp\left[-4\ln 2\frac{(\omega-\omega_0)^2}{\Delta\omega_G^2}\right], \tag{4}$$

with linewidth

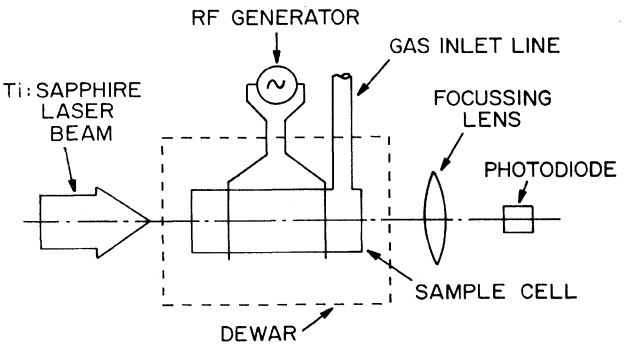

FIG. 1. Schematic diagram of the apparatus.

$$\Delta\omega_G=\frac{2\omega_0}{c}\left[\frac{2k_BT\ln 2}{M}\right]^{1/2}, \tag{5}$$

and a Lorentzian $g_L(\omega,\omega_0)$ representing homogeneous broadening due to spontaneous emission and collisional P-state mixing,

$$g_L(\omega,\omega_0)=\frac{1}{\pi}\frac{\Delta\omega_L/2}{(\omega_0-\omega)^2+(\Delta\omega_L/2)^2}, \tag{6}$$

with linewidth

$$\Delta\omega_L=2(A+k_mN)=2(A+\sigma_m\bar{v}N), \tag{7}$$

where ω_0 is the transition frequency at line center, ω the laser frequency, k_B the Boltzmann constant, T the absolute temperature, M the helium mass, c the velocity of light, A ($\cong 10^7$ s^{-1}) the $2\,^3P_J \rightarrow 2\,^3S_1$ spontaneous emission rate, N the helium number density, $\bar{v}$ the mean relative collision velocity, and k_m and σ_m the rate coefficient and thermally averaged cross section, respectively, for collisional mixing.

The measured line shape, represented by the convolution integral

$$g_v(\omega,\omega_0)=\int_{-\infty}^{\infty}g_L(\omega,\Omega)g_G(\Omega,\omega_0)d\Omega \tag{8}$$

and commonly called the Voigt function, is easily decomposed by a simple graphical analysis procedure to yield the widths $\Delta\omega_G$ and $\Delta\omega_L$ of the Gaussian and Lorentzian components [20,21]. The rate coefficients and thermally averaged cross sections are obtained from the extracted values of $\Delta\omega_L$ using Eq. (7).

Absorption profiles for He($2\,^3S_1$)$\rightarrow$He($2\,^3P_J$) transitions were measured at temperatures of 300, 77, and 4.2 K, for sample gas densities in the range $\sim 10^{17}$ cm^{-3} to $\sim 5\times 10^{18}$ cm^{-3}. The intensity of the rf discharge was adjusted to the lowest sustainable level to avoid significant heating and to ensure that the absorption profiles were measured using optically-thin samples. The absorption at line center was typically $\sim 10\%$. Laser frequency drift during absorption scans, however, can distort the measured profiles, and changes in laser intensity can cause baseline drift. An absorption profile was deemed acceptable only if it exhibited little or no baseline drift, if upon analysis it yielded a Gaussian linewidth component $\Delta\omega_G$ within 10% of that calculated using Eq. (5), and if the values of $\Delta\omega_L$ and $\Delta\omega_G$ extracted from near-wing and far-wing portions of the spectrum agreed to within 15%.

A typical $2\,^3S_1 - 2\,^3P_{1,2}$ absorption profile, obtained at a temperature of 4.2 K and gas density of 1.25×10^{18} cm^{-3}, is shown in Fig. 2. Values of k_m and σ_m obtained from such data are presented in Table I. The uncertainties are estimated to be $\lesssim \pm 25\%$ at 300 and 77 K, and $\lesssim \pm 10\%$ at 4.2 K.

The rate coefficient for P-state mixing decreases slowly with decreasing temperature, and the cross sections are consistent with the $T^{-1/3}$ dependence predicted by Langevin "spiraling-orbit" theory for an r^{-6} interaction potential, superimposed on a hard-sphere cross section of about 6×10^{-15} cm^2 [22]. The cross section measured at

TABLE I. Measured rate coefficients and thermally averaged cross sections for P-state mixing, reaction (2). $\bar{v}=(16k_BT/\pi M)^{1/2}$ is the average relative speed.

Temperature (K)	k_m (10^{-10} cm^3 s^{-1})	$\bar{v}$ (10^5 cm s^{-1})	σ_m (10^{-16} cm^2)
300	18±5	2.06	87±22
			68±3[a]
77	12±3	1.04	115±29
4.2	4.5±0.5	0.24	185±19

[a]Reference [23].

300 K is in satisfactory agreement with the value $(68\pm3)\times10^{-16}$ cm^2 reported previously by Schearer [23].

To obtain rate constants for three-body conversion, reaction (3), the laser was tuned to the center of one of the $2\,^3S_1-2\,^3P_J$ transitions and the decay of the radiation-coupled $2\,^3S_1/2\,^3P_J$ population in the late afterglow of a pulsed rf discharge measured by observing the time dependence of the absorption of the laser radiation. The discharge was excited by low-power rf pulses of ~100-μs duration with a pulse repetition frequency between 10 and 150 Hz depending on sample density and temperature. The use of low-power pulses assured that the fractional absorption of the laser-probing radiation during the period over which data were recorded was small: $\lesssim5\%$ for $T\gtrsim200$ K and $\lesssim2\%$ at lower temperatures.

In our earlier study of the temperature dependence for conversion of He($2\,^3S$) metastable atoms to $He_2(a\,^3\Sigma_u^+)$ molecules, it was demonstrated that at high helium densities diffusion can be neglected and that in the late afterglow the only significant He($2\,^3S$) loss mechanism was three-body conversion, reaction (1) [16]. The He($2\,^3S$) concentration during the time interval over which data were recorded was well described by the relation

$$\frac{dS}{dt}=-k_SN^2S\ , \tag{9}$$

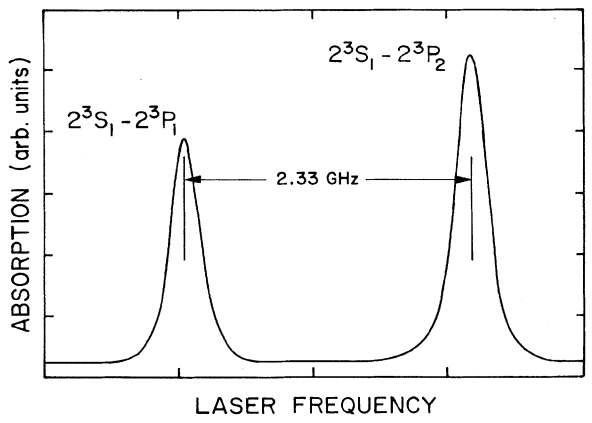

FIG. 2. Absorption profiles associated with the He($2\,^3S_1$)-He($2\,^3P_1$) and He($2\,^3S_1$)-He($2\,^3P_2$) transitions at 4.2 K, for helium gas density 1.25×10^{18} cm^{-3}.

where S and N ($S\ll N$) are the densities of metastable $2\,^3S_1$ and ground-state $^1S_0$ helium atoms respectively, and k_S is the rate constant for reaction (1). The He($2\,^3S_1$) volume loss rate, $\alpha_S=k_SN^2$, was determined by monitoring the absorption of $2\,^3S_1-2\,^3P_J$ resonance radiation from a conventional helium discharge lamp. Atoms excited to $2\,^3P_J$ levels by the probing radiation returned to the $2\,^3S_1$ state by spontaneous emission with lifetime $\sim10^{-7}$ s. The intensity provided by the lamp was sufficiently low that the fraction of the excited atoms in $2\,^3P_J$ levels at any instant was less than 10^{-6} and their collisions thus provided a negligible contribution to the measured He($2\,^3S_1$) loss rate.

The Ti:sapphire laser can produce much higher fractional $2\,^3P_J$ populations and their collisions become important. As demonstrated by the simple kinetic model presented in the Appendix, measurements of the volume decay rate of the radiation-coupled $2\,^3S_1/2\,^3P_J$ population in the late afterglow as a function of laser intensity and gas density can yield the rate coefficient $k_P(T)$ for three-body conversion, reaction (3). Tests verified that the excited atom population decayed exponentially and that the measured decay rate was independent of the rf pulse power. The laser radiation uniformly illuminated the entire sample cell to minimize possible effects associated with local variations in He($2\,^3S_1$) density.

The only significant processes for destruction of He($2\,^3S_1$) and He($2\,^3P_J$) atoms in the late afterglow are reactions (1) and (3), and diffusion to the container walls. As shown in the Appendix, the common volume decay rate α of the radiation-coupled states is given by

$$\alpha=\frac{(A+R)\left[k_SN^2+\dfrac{D_S}{\Lambda N^2}\right]+R\dfrac{g_{P_J}}{g_S}\left[k_PN^2+\dfrac{D_P}{\Lambda^2N}\right]}{A+R\left[1+\dfrac{g_{P_J}}{g_S}\right]}\ , \tag{10}$$

where g_S and g_{P_J} are the statistical weights of the two coupled states, D_S and D_P the diffusion coefficients of He($2\,^3S_1$) and He($2\,^3P_J$) atoms normalized to unit helium gas number density, Λ the lowest mode diffusion length of the sample cell, and R the stimulated emission rate given by

$$R(\omega)=\frac{\lambda^2}{8\pi}Ag_v(\omega,\omega_0)\frac{I(\omega)}{\hbar\omega} \tag{11}$$

for transition wavelength λ and radiation intensity $I(\omega)$. The line-shape function $g_v(\omega,\omega_0)$ is the Voigt function [Eq. (8)].

In the limit $R\ll A$, and if the laser is tuned to the center of a particular $2\,^3S_1-2\,^3P_J$ transition, i.e., $\omega=\omega_0$, the decay rate α is related to the intensity of the exciting radiation by

$$\frac{d\alpha}{dI(\omega_0)} = \frac{g_{P_J}}{g_S}\frac{\lambda^2}{8\pi\hbar\omega_0} g_v(\omega_0,\omega_0) \times \left[(k_P - k_S)N^2 + \frac{(D_P - D_S)}{\Lambda^2 N}\right] . \quad (12)$$

Typical data showing the dependence of the measured decay rates α on laser intensity $I(\omega_0)$ are presented in Fig. 3. These data were obtained with the laser tuned to the $2\,^3S_1 - 2\,^3P_2$ transition at a fixed helium sample density $N = 3.23\times10^{17}$ cm^{-3} for several different sample temperatures in the liquid-helium range. The slopes $d\alpha/dI(\omega_0)$ are seen to be strongly dependent on sample temperature. As expected, the measured slopes were five times smaller with the laser tuned to the $2\,^3S_1 - 2\,^3P_0$ transition ($g_{P_2}=5$, $g_{P_0}=1$). The small nonzero intercept in Fig. 3 is due to He($2\,^3S_1$) losses by diffusion to the walls of the sample cell. [See Appendix, Eq. (A10). The rate coefficient k_S is negligibly small at liquid-helium temperatures.]

Values of $d\alpha/dI(\omega_0)$ measured over a wide range of helium densities and temperatures revealed no evidence of significant contributions from the diffusion term $(D_P - D_S)/\Lambda^2 N$ in Eq. (12). Indeed, at all temperatures $d\alpha/dI(\omega_0)$ was found to be simply proportional to $N^2 g_v(\omega_0,\omega_0)$. This is illustrated in Fig. 4 where the density dependence of $d\alpha/dI(\omega_0)$ is plotted at 77 and 300 K. The shaded regions are proportional to $N^2 g_v(\omega_0,\omega_0)$, and encompass the uncertainties in $g(\omega_0,\omega_0)$ that result from uncertainties in the measured values of k_m. [The procedure employed to calculate the density and temperature dependence of $g_v(\omega,\omega_0)$ is described in the Appendix and representative values of $g_v(\omega_0,\omega_0)$ for the present experimental conditions can be obtained using Table II.] For comparison, the dashed line in Fig. 4 shows a simple N^2 dependence. Because the diffusion term in Eq. (12) is negligible, the measured slopes $d\alpha/dI(\omega_0)$ are directly related to $(k_P - k_S)$, i.e., k_P since $k_P \ll k_S$.

The measured reaction rate coefficients $k_P(T)$ are presented in Fig. 5. These depend linearly on T^{-1} and

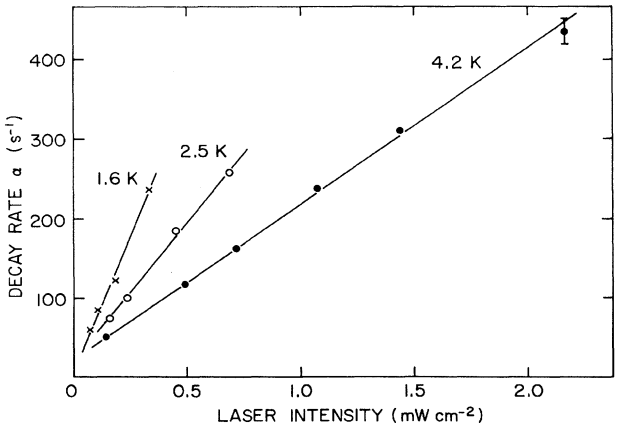

FIG. 3. Dependence of the measured decay rates α on laser intensity at temperatures of 4.2, 2.5, and 1.6 K for a helium density of 3.23×10^{17} cm^{-3}.

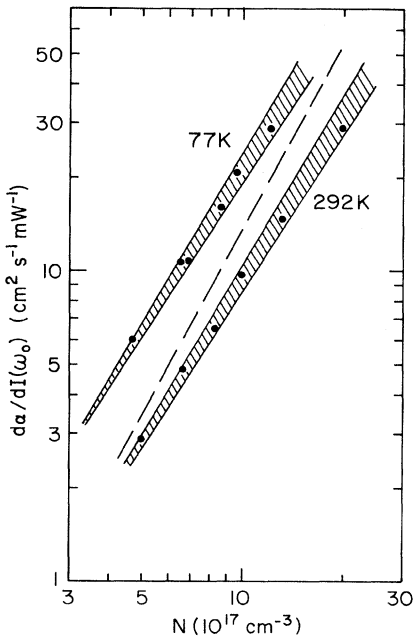

FIG. 4. Dependence of $d\alpha/dI(\omega_0)$ on helium density at temperatures of 292 and 77 K. The dots are experimental data and the shaded regions are proportional to $N^2 g_v(\omega_0,\omega_0)$ (see text). The dashed line shows a simple N^2 dependence.

are accurately represented by the function

$$k_P(T) = (2.5 + 267T^{-1})\times10^{-32}\ \text{cm}^6\text{s}^{-1} , \quad (13)$$

shown as the solid line in Fig. 5. The observed T^{-1} dependence is consistent with the predictions of a simple model based on detailed balancing and kinetic theory developed earlier by Niles and Robertson [24] to explain their experiments which showed that the rate coefficient for conversion of He^+ ions to molecular $He_2{}^+$ ions via the three-body reaction

$$He^+ + 2He(1\,^1S_0) \rightarrow He_2{}^+ + He(1\,^1S_0) \quad (14)$$

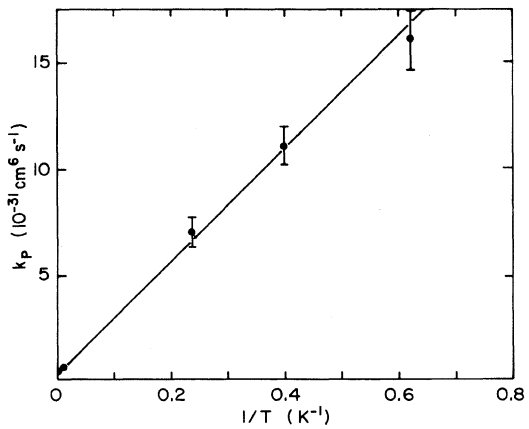

FIG. 5. Rate coefficient $k_P(T)$ for reaction (3) as a function of $1/T$. ⧫, experimental data; ——, Eq. (13).

also varies at T^{-1}.

The magnitude and temperature dependence of k_P is in marked contrast to that of k_S, the corresponding rate coefficient for reaction (1), reproduced in Fig. 6 [16]. While reaction (3) is clearly exothermic, the rapid decrease in k_S with decreasing temperature shows that reaction (1) is thermally activated. The temperature-dependence of k_S is well represented by the function

$$k_S(T)=T[8.7\exp(-750/T)+0.41\exp(-200/T)] \times 10^{-36}\ \mathrm{cm^6\,s^{-1}}, \quad (15)$$

shown as the solid line in Fig. 6 [16]. The first term, which dominates at high temperatures, corresponds to an activation energy 750±70 K (64±4 meV) equal (as expected) to the known height of the He($2\,^3S_1$)–He($1\,^1S_0$) repulsive barrier [10–13]. However, at lower temperatures k_S is much greater than expected, suggesting that for certain reaction geometries the barrier height along the He($2\,^3S_1$)–He($1\,^1S_0$) reaction path is significantly reduced by the presence of the second He($1\,^1S_0$) atom [16]. This is reflected in the second term in Eq. (15), which suggests that at low temperatures the reaction can be adequately characterized by an effective (or average) activation energy of 200±20 K (17±2 meV). It is interesting that, while k_P varies as T^{-1}, the prefactor in Eq. (15) for k_S is T. This was demonstrated by measurements showing that values of k_S for the light ^{3}He isotope are ~33% higher than those for ^{4}He, reflecting the higher thermal velocity of the lighter isotope [16].

The observation that reaction (3) is exothermic can be reconciled with earlier studies suggesting that He($2\,^3P_J$) atoms tend to repel ground-state atoms in liquid helium by remembering that the He($2\,^3P_J$)–He($1\,^1S_0$) exchange repulsion will be small for collisions in which the internuclear axis is in the nodal plane of the $2p$-electron orbital, and is apparently insufficient to produce a significant potential barrier [14,15]. Thus, in order for reaction (3) to proceed, it would seem necessary that at least one of the two He($1\,^1S_0$) atoms approaches the He($2\,^3P_J$) atom in (or close to) the $2p$ nodal plane.

Reactions (1) and (3) are among the most fundamental three-body reactions that can be studied in the laboratory over an extended temperature range. Theoretical efforts to determine the pertinent potential-energy surfaces would enable molecular dynamics calculations for quantitative comparisons with the results presented here and in Ref. [16].

The authors are grateful to N. F. Lane for valuable discussions regarding helium interaction potentials and bubble states of He($2\,^3S_1$) and He($2\,^3P_J$) atoms in liquid helium. This research is supported by National Science Foundation Grant No. PHY-9021196 and by the Robert A. Welch Foundation.

APPENDIX: BEHAVIOR OF A RADIATIVELY-COUPLED $2\,^3S_1/2\,^3P_J$ POPULATION

The Ti:sapphire laser excites transitions between the helium $2\,^3S_1$ level and one of the $2\,^3P_J$ levels shown in the partial term diagram Fig. 7 [25], and is also used to monitor, through absorption, their combined populations in the afterglow of a pulsed rf discharge. In the early afterglow, immediately following the rf pulse, significant production of He($2\,^3S_1$) atoms can occur as the result of He($2\,^1S_0$) to He($2\,^3S_1$) conversion in superelastic collisions with electrons. An important loss channel is Penning ionization in collisions between pairs of excited atoms that results in ionization of one and deexcitation of the other. Both these processes can be neglected in the late afterglow where He($2\,^1S_0$) to He($2\,^3S_1$) conversion is essentially complete and the excited atom density is low [3,4],[16]. Thus, a simple two-level model can provide an adequate description of the time evolution of the optically coupled $2\,^3S_1/2\,^3P_J$ population in the late afterglow, provided that the radiation field is sufficiently weak that the $2\,^3P_J$–$2\,^3S_1$ spontaneous emission rate is much greater than that for stimulated emission. The He($2\,^3S_1$) and He($2\,^3P_J$) production and loss mechanisms, and their associated rates, are as indicated in Fig. 8. The symbols

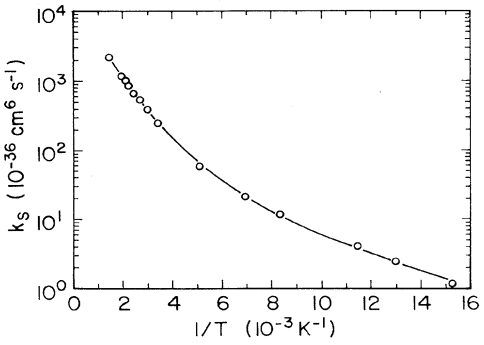

FIG. 6. Rate coefficient $k_S(T)$ for reaction (1) as a function of $1/T$. ○, experimental data; ——, Eq. (15).

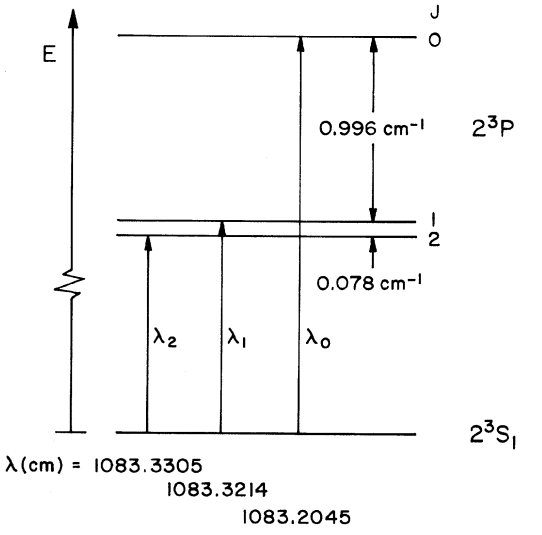

FIG. 7. Partial term diagram showing the levels of interest in this work.

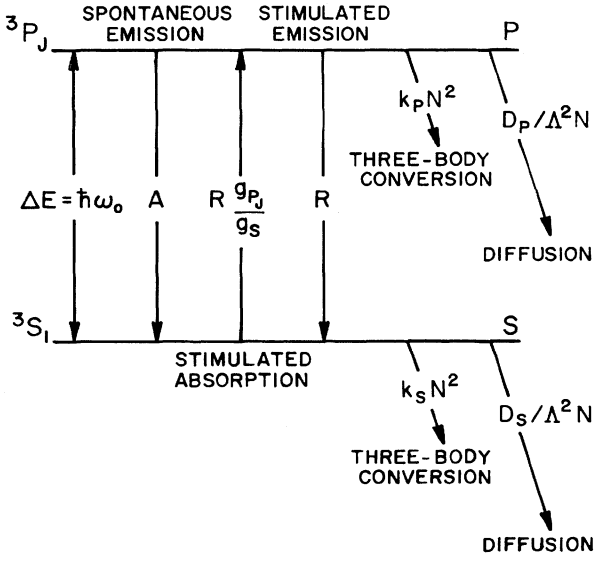

FIG. 8. Simple two-level model used in data analysis. The $2\,^3S_1$ and $2\,^3P_J$ production and loss processes and rates are as indicated.

used in the figure and the following text are defined as follows: N, number density of ground-state He($1\,^1S_0$) atoms; S,P, number densities of He($2\,^3S_1$) and He($2\,^3P_J$) atoms; g_S,g_{P_J}, statistical weights of the $2\,^3S_1$ and $2\,^3P_J$ states; D_S,D_P, diffusion coefficients for He($2\,^3S_1$) and He($2\,^3P_J$) atoms normalized to unit helium number density; Λ, lowest mode diffusion length of the sample cell; k_S,k_P, rate coefficients for three-body conversion, i.e. reactions (1) and (3); ω, laser frequency; ω_0,λ_0, transition frequency and wavelength; $I(\omega)$, intensity of radiation field at frequency ω; A, He($2\,^3P_J$) spontaneous emission rate, $\cong 10^7$ s^{-1}; R, He($2\,^3P_J$) stimulated emission rate; and $g_v(\omega,\omega_0)$, absorption (Voigt) line-shape function [Eq. (8)].

The differential equations that govern the decay of the $^3S_1$ and ^3P_J populations in the late afterglow are

$$\frac{dS}{dt}=-\left[R\frac{g_{P_J}}{g_S}+\frac{D_S}{N\Lambda^2}+k_SN^2\right]S+(R+A)P\ , \tag{A1}$$

$$\frac{dP}{dt}=R\frac{g_{P_J}}{g_S}S-\left[R+A+\frac{D_P}{N\Lambda^2}+k_PN^2\right]P\ . \tag{A2}$$

These coupled equations have solutions of the form $S,P\sim e^{-\alpha t}$ and yield two rate coefficients. The first,

$$\alpha'=A+R\left[1+\frac{g_{P_J}}{g_S}\right]\geq 10^7\ \text{s}^{-1}\ , \tag{A3}$$

characterizes the rate at which the S and P populations equilibrate with one another in the presence of the radiation field. The second,

$$\alpha=\frac{(A+R)\left[k_SN^2+\frac{D_S}{\Lambda N^2}\right]+R\frac{g_{P_J}}{g_S}\left[k_PN^2+\frac{D_P}{\Lambda^2N}\right]}{A+R\left[1+\frac{g_{P_J}}{g_S}\right]}$$

$$\lesssim 10^4\ \text{s}^{-1}\ , \tag{A4}$$

is the common decay rate of the coupled $^3S_1/^3P_J$ population that is measured in the experiment. Because $\alpha\ll\alpha'$, the $^3S_1$ and ^3P_J populations are in quasiequilibrium with one another and the ratio of their densities is

$$\frac{P}{S}=\frac{g_{P_J}}{g_S}\left[1+\frac{A}{R}\right]^{-1}\ . \tag{A5}$$

In the limit $R\gg A$, $P/S=g_{P_J}/g_S$ and

$$\alpha=\frac{g_S}{g_S+g_P}\left[k_SN^2+\frac{D_S}{\Lambda^2N}\right]+\frac{g_{P_J}}{g_S+g_P}\left[k_PN^2+\frac{D_P}{\Lambda^2N}\right] \tag{A6}$$

is simply a weighted linear combination of the $^3S_1$ and ^3P_J decay rates. The two-level model developed here is, however, inadequate for interpreting experiments that utilize intense radiation fields because it does not take into account P-state mixing which transfers laser-excited ^3P_J atoms to other ^3P_J levels that can only decay by spontaneous emission. However, in the limit $R\ll A$, $P/S=(g_{P_J}/g_S)R/A$, so $S\gg P$ and α is given to a good approximation by

$$\alpha=\left[k_SN^2+\frac{D_S}{\Lambda^2N}\right]+\frac{g_{P_J}}{g_S}\left[(k_P-k_S)N^2+\frac{(D_P-D_S)}{\Lambda^2N}\right]\frac{R}{A}\ . \tag{A7}$$

If the laser is tuned to the center of a particular $^3S_1$-^3P_J transition, the stimulated emission rate is given by

$$R=\frac{\lambda^2}{8\pi}g_v(\omega_0,\omega_0)\frac{I(\omega_0)}{\hbar\omega_0}A\ , \tag{A8}$$

and the decay rate α is related to the intensity of the exciting radiation by

$$\frac{d\alpha}{dI(\omega_0)}=\frac{g_{P_J}}{g_S}\frac{\lambda^2}{8\pi\hbar\omega_0}g_v(\omega_0,\omega_0)\times\left[(k_P-k_S)N^2+\frac{(D_P-D_S)}{\Lambda^2N}\right]\ . \tag{A9}$$

If no laser radiation is present, $I(\omega_0)=0$ and α is given by

$$\alpha(I=0)=k_SN^2+\frac{D_S}{\Lambda^2N}\ , \tag{A10}$$

which is simply the decay rate appropriate to a pure $2\,^3S_1$ population. The two-level model is adequate in the

TABLE II. Representative values of $\mathrm{Re}\{Z(\zeta)\}=(\Delta\omega_G/0.939)g_v(\omega_0,\omega_0)$.

T (K)	N (10^{16} atoms cm^{-3})	$\Delta\omega_G$ (ns^{-1})	$\Delta\omega_L$ (ns^{-1})[a]	$\mathrm{Re}\{Z(\zeta)\}$[b]
292	50	10.6	1.8	0.86±0.03
	100		3.6	0.75±0.05
	150		5.4	0.66±0.06
	200		7.2	0.59±0.07
77	25	5.44	0.62	0.90±0.03
	50		1.2	0.82±0.04
	75		1.8	0.75±0.05
	100		2.4	0.69±0.06
	125		3.0	0.64±0.07
4.2	15	1.27	0.16	0.89±0.01
	30		0.29	0.82±0.02
2.5	15	0.98	0.14	0.88±0.01
	30		0.26	0.79±0.02
1.6	15	0.79	0.13	0.86±0.02
	30		0.24	0.77±0.03

[a]Calculated from Eq. (7) using Table I. Values of k_m at 2.5 and 1.6 K are estimated from the relation $\sigma_m=[5.8+21.5T^{-1/3}]\times10^{-15}$ cm^2, which fits the data in Table I and is consistent with Langevin theory. Estimated uncertainties are ±25% at 292 and 77 K, ±10% at 4.2 K and below.
[b]Reference [26].

$R \ll A$ limit because the great majority of the excited $2\,^3P_J$ atoms return to the $2\,^3S_1$ state via spontaneous emission with rate A, which is common to all three J levels. Thus collisional mixing is of little consequence to the kinetics.

In order to extract rate constants for three-body conversion from measured decay rates α, it is necessary to evaluate the integral in Eq. (8) for the Voigt line-shape function, which depends on both temperature and the gas density because of collisional mixing. However, the line-shape function can be determined using the known rate constants k_m for collisional mixing and the integral evaluated in terms of the tabulated form [26]

$$Z(\zeta)=\frac{i}{\pi}\int_{-\infty}^{\infty}\frac{e^{-t^2}dt}{\zeta-t},\quad \mathrm{Im}Z>0\ , \tag{A11}$$

where

$$\zeta=1.665\left[\frac{\omega_0-\omega}{\Delta\omega_G}\right]+i\left[0.833\frac{\Delta\omega_L}{\Delta\omega_G}\right], \tag{A12}$$

by reexpressing Eq. (8) in complex form as

$$g_v(\omega,\omega_0)=\mathrm{Im}\{\tilde{g}_v(\omega,\omega_0)\}$$
$$=\mathrm{Im}\left\{\int_{-\infty}^{\infty}\tilde{g}_L(\omega,\Omega)g_G(\Omega,\omega_0)d\Omega\right\}, \tag{A13}$$

where

$$\tilde{g}_L(\omega,\Omega)=\frac{1}{\pi}\frac{1}{(\Omega-\omega)+i\left[\frac{\Delta\omega_L}{2}\right]} \tag{A14}$$

is the complex Lorentzian. For $\omega=\omega_0$, $\zeta=i(0.833\Delta\omega_L/\Delta\omega_G)$ and

$$g_v(\omega_0,\omega_0)=\frac{0.939}{\Delta\omega_G}\mathrm{Re}\{Z(\zeta)\}\ . \tag{A15}$$

Representative values of $\mathrm{Re}\{Z(\zeta)\}$ appropriate to the experimental analysis are presented in Table II.

[1] R. A. Buckingham and A. Dalgarno, Proc. R. Soc. London Ser. A **213**, 327 (1952).
[2] R. A. Buckingham and A. Dalgarno, Proc. R. Soc. London Ser. A **213**, 502 (1952).
[3] A. V. Phelps and J. P. Molnar, Phys. Rev. **89**, 1202 (1953).
[4] A. V. Phelps, Phys. Rev. **99**, 1307 (1955).
[5] F. D. Colegrove, L. D. Schearer, and G. K. Walters, Phys. Rev. **135**, A353 (1964).
[6] J. Dupont-Roc, M. Leduc, and F. Laloë, Phys. Rev. Lett. **27**, 467 (1971).
[7] S. D. Rosner and F. M. Pipkin, Phys. Rev. A **5**, 1909 (1972).
[8] W. A. Fitzsimmons, N. F. Lane, and G. K. Walters, Phys. Rev. **174**, 193 (1968).
[9] A. P. Hickman and N. F. Lane, Phys. Rev. A **10**, 444 (1974).
[10] B. Brutschy and H. Haberland, Phys. Rev. A **19**, 2232 (1979).
[11] R. M. Jordan, H. R. Siddiqui, and P. E. Siska, J. Chem. Phys. **84**, 6719 (1986).
[12] D. D. Konowalow and B. H. Lengsfield III, J. Chem. Phys. **87**, 4000 (1986).

[13] D. R. Yarkony, J. Chem. Phys. **90**, 7164 (1989).
[14] W. S. Dennis, E. Durbin, Jr., W. A. Fitzsimmons, O. Heybey, and G. K. Walters, Phys. Rev. Lett. **23**, 1083 (1969).
[15] A. P. Hickman and N. F. Lane, Phys. Rev. B **12**, 3705 (1975).
[16] A. Köymen, F.-C. Tang, X. Zhao, F. B. Dunning, and G. K. Walters, Chem. Phys. Lett. **168**, 405 (1990).
[17] G. H. Rutherford, J. M. Ratliff, J. G. Lynn, F. B. Dunning, and G. K. Walters, Rev. Sci. Instrum. **61**, 1460 (1990).
[18] See, for example, 7th International Conference on Polarization Phenomena in Nuclear Physics (Paris) [J. Phys. (Paris) Colloq. **51**, C-6 (1990)].
[19] See, for example, *Spin Polarized Quantum Systems,* edited by S. Stringari (World Scientific, Singapore, 1989).
[20] H. C. van de Hulst and J. J. M. Reesinck, Astrophys. J. **106**, 121 (1947).
[21] J. T. Davies and J. M. Vaughan, Astrophys. J. **137**, 1302 (1963).
[22] E. W. McDaniel, *Atomic Collisions* (Wiley, New York, 1989), p. 86ff.
[23] L. D. Schearer, Phys. Rev. **160**, 76 (1967).
[24] F. E. Niles and W. W. Robertson, J. Chem. Phys. **42**, 3277 (1965).
[25] S. Bashkin and J. O. Stoner, Jr., *Atomic Energy Levels and Grotrian Diagrams, Vol. I* [North-Holland, Amsterdam (1975)].
[26] *Handbook of Mathematical Functions,* edited by M. Abramowitz and I. A. Stegun, Natl. Bur. Stand. (U.S.) Appl. Math. Ser. No. 55 (U.S. GPO, Washington, DC, 1964), p. 297ff.